

Article

Effect of Reducing Agent on Solution Synthesis of $\text{Li}_3\text{V}_2(\text{PO}_4)_3$ Cathode Material for Lithium Ion Batteries

Ali Yaghtin ^{1,2,3}, Seyyed Morteza Masoudpanah ^{2,*} , Masood Hasheminasari ², Amirhossein Salehi ^{1,2,3}, Dorsasadat Safanama ³, Chong Kim Ong ⁴, Stefan Adams ³ and Mogalahalli V. Reddy ^{1,3,5,*} 

¹ Department of Physics, National University of Singapore, Singapore 117542, Singapore; ali.yaghtin93@gmail.com (A.Y.); amirhsalehi.23@gmail.com (A.S.)

² School of Metallurgy and Materials Engineering, Iran University of Science and Technology (IUST), Narmak, Tehran 13114-16846, Iran; mhashemi@iust.ac.ir

³ Department of Materials Science and Engineering, National University of Singapore, Singapore 117575, Singapore; mseds@nus.edu.sg (D.S.); mseasn@nus.edu.sg (S.A.)

⁴ Department of Mathematics, Xiamen University Malaysia, Jalan Sunsuria, Bandar Sunsuria, Sepang 43900, Selangor, Malaysia; ckong@xmu.edu.my

⁵ Centre of Excellence in Transportation Electrification and Energy Storage (CETEES), Varennes, QC 1806, Canada

* Correspondence: masoodpanah@iust.ac.ir (S.M.M.); MogalahalliVenkatesh.VenkatashamyReddy@ireq.ca or MogalahalliVenkatesh.VenkatashamyReddy@hydroquebec.com (M.V.R.)

Academic Editors: Cesar Augusto Correia de Sequeira and Gregorio F. Ortiz
Received: 3 July 2020; Accepted: 12 August 2020; Published: 17 August 2020



Abstract: In this study, $\text{Li}_3\text{V}_2(\text{PO}_4)_3$ (LVP) powders are prepared by a solution synthesis method. The effects of two reducing agents on crystal structure and morphology and electrochemical properties are investigated. Preliminary studies on reducing agents such as oxalic acid and citric acid, are used to reduce the vanadium (V) precursor. The oxalic acid-assisted synthesis induces smaller particles (30 nm) compared with the citric acid-assisted synthesis (70 nm). The LVP powders obtained by the oxalic acid exhibit a higher specific capacity (124 mAh g^{-1} at 1C) and better cycling performance (122 mAh g^{-1} following 50 cycles at 1C rate) than those for the citric acid. This is due to their higher electronic conductivity caused by carbon coating and downsizing the particles. The charge-discharge plateaus obtained from cyclic voltammetry are in good agreement with galvanostatic cycling profiles.

Keywords: $\text{Li}_3\text{V}_2(\text{PO}_4)_3$; solution synthesis method; reducing agent; electrochemical properties

1. Introduction

Lithium ion batteries (LIBs) are promising electrochemical power sources that are used in portable electronics and hybrid electric vehicles because of their high energy density [1,2]. Among the cathode materials, vanadium-based oxides are one of the important electrode materials that are studied due to their variable $\text{V}^{3+,4+,5+}$ oxidation state. Early work on a vanadium-based oxide, $\text{Li}_x\text{V}_2\text{O}_5$, was conducted in 1979 by Dickeson et al. [3], and further details on the early history of lithium batteries have been summarized by Reddy et al. [4]. More recently, various studies have been carried out on vanadium-based cathodes with different crystal structures: triclinic [5–10], tetragonal [11], and orthorhombic [12,13]. Furthermore, $\text{Li}_3\text{V}_2(\text{PO}_4)_3$ (LVP) has been studied for its potential for practical applications in LIBs due to its unique properties such as thermal stability and high theoretical specific capacity [14–16]. The covalence P-O bonds and 3D solid framework of $(\text{PO}_4)^{3-}$ anions guarantee both good dynamic and thermal stabilities of LVP cathode [17]. The LVP has also a high theoretical

specific capacity of 197 mAh g⁻¹ and a moderate working voltage [18]. LVP has two crystal structures; rhombohedral and monoclinic structures, in which the monoclinic LVP shows a higher specific capacity due to the intercalation/de-intercalation of three Li ions per formula unit in stable phase transitions from Li₃V₂(PO₄)₃ to V₂(PO₄)₃ [19]. The monoclinic LVP has specific capacities of 133 and 197 mAh g⁻¹ as a function of applied electrochemical windows of 3.0–4.3 and 3.0–4.8 V vs. Li⁺/Li, on the basis of the de/intercalation of two and three Li⁺ ions, respectively [20]. However, the pristine LVP exhibits poor rate performance caused by its low electronic conductivities, which can be mitigated by downsizing, carbon coating, and aliovalent doping [21–23].

The wet-chemical synthesis of LVP is generally based on the reduction of cost-efficient V(V) precursors V₂O₅ and NH₄VO₃, to V(IV) species by organic reducing agents such as oxalic acid, citric acid, glucose, and sucrose [24–26]. The V(IV) is then reduced to V(III) at high temperatures during the calcination process for the formation of LVP. The organic reductants can function both as a chelating agent and a carbon source, affecting the physiochemical properties of obtained LVP powders [24]. No comparison of the role of reducing agent type on the electrochemical properties has been performed thus far. To clarify the comparison, the oxalic acid and citric acid were used as reducing agents. Furthermore, the solution method was selected for synthesis of LVP/C composite material due to factors such as simplicity, versatility, and time- and energy-efficiency [27–29]. The solution method is based on dissolving the metal precursors together with a suitable organic agent (such as CTAB) in water as a solvent. The precursor solution is then dried and decomposed at low temperatures (<350 °C). To obtain the final product, the dried gel is calcined at high temperatures (700–900 °C) [30]. The thermal decomposition rate, organic agents, calcination temperatures, and times, etc. are crucial factors in the powder characteristics.

In this work, the phase, morphology, and electrochemical properties of LVP powders were studied as a function of the type of reducing agent. The smaller particles and higher carbon coating of the LVP prepared by the oxalic acid led to higher capacity and cyclic stability, despite their lower specific surface area.

2. Experimental Procedure

2.1. Synthesis of Li₃V₂(PO₄)₃ Powders

V₂O₅ (Aldrich, Darmstadt, Germany), oxalic acid, H₂C₂O₄, (Aldrich), citric acid, C₆H₈O₇ (Aldrich), NH₄H₂PO₄, and Li₂CO₃ were used as starting materials. V₂O₅, NH₄H₂PO₄, Li₂CO₃ were in a molar ratio of 1:3:1.5. 0.4 mmol cetyltrimethylammonium bromide (CTAB; (C₁₆H₃₃)N(CH₃)₃]⁺ Br⁻) was successively dissolved into 50 mL of deionized water at 80 °C under vigorous stirring. The precursor solution was initially dried and then preheated at 350 °C for 20 min in a box furnace under air atmosphere. The powders obtained were finally calcined at 700 and 800 °C for 3 and 6 h under an argon atmosphere in a tube furnace (CarbolYTE, Hope Valley, UK), with a heating rate of 3 °C/min.

2.2. Material Characterization Methods

Thermal analysis was performed using a STA 503 (BäHR, Hüllhorst, Germany) simultaneous thermal analyzer under air atmosphere at a heating rate of 5 °C min⁻¹. The phases and structure of the LVP powders were analyzed using a D8 ADVANCE (Bruker, Kanagawa, Japan) X-ray powder diffraction (XRD) instrument with Cu Kα (λ = 1.54060 Å) radiation in the 2θ range of 10–60° at the scan rate of 0.04°/0.5 s. The morphology and microstructure of the powders were analyzed using a VEGA II (TESCAN, Brno, Czech Republic) scanning electron microscopy (SEM) device in the backscattered-electron mode at 15 kV and JEM-2010F (JEOL, Tokyo, Japan) transmission electron microscopy (TEM) apparatus at 200 kV. The textural properties of the composites were characterized using their N₂ adsorption/desorption isotherms, which were obtained employing a Tristar 3000 (Micromeritics, Norcross, GA, USA) porosity analyzer. A P50C0R10 (Takram, Gilan, Iran) Raman spectroscope with a Nd:YAG laser was used to analyze the carbon coating. An X-ray photoelectron

spectrometer (XPS) was used for detection of state of element using an AXIS ultra DLD spectrometer (Kratos Analytica, Manchester, UK) equipped with a monochromatic Al-K α radiation. Further details of instrumentation are reported elsewhere [31]. The XRD, Raman, TGA, SEM, TEM, and XPS experiments were performed on the LVP/C samples calcined at 800 °C.

2.3. Electrochemical Characterization

The electrochemical properties were characterized in 2016 type coin cells. The LVP, polyvinylidene fluoride (PVDF), and Super-P carbon black in 70:15:15 wt.% ratio, respectively, were firstly mixed in *N*-methyl-2-pyrrolidone. The slurry was coated on aluminum foil and then dried in a vacuum oven overnight. The coated foil was cut into pieces of circular shape with a diameter of 16 mm. The working electrode had approximately 2.5 mg cm⁻² of active material. The lithium metal as a counter/reference electrode, glass fiber as a separator, and 1M LiPF₆ (EC and DMC *v/v* = 1:1) solution as the electrolyte were used to assemble a coin cell in an argon-filled glove box (MBraum, Bayern, Germany). Galvanostatic charge-discharge experiments (Bitrode, USA battery tester, St. Louis, MO, USA) and cyclic voltammetry (Solartron-1470, Cambridge, UK) were performed in the voltage range of 3.0 to 4.8 V. Electrochemical impedance spectroscopy (EIS) was carried out on a Solartron 1260A system. Further details of instrumentation are reported elsewhere [32].

3. Results and Discussion

Figure 1 shows the XRD patterns of the samples prepared by oxalic and citric acids as the reducing agents following calcination at 800 °C for 6 h. The indexed diffraction peaks are related to the monoclinic LVP structure with the space group of P21/n (PDF no. 01-072-7074). The calculated lattice parameters of LVP are *a* = 8.612, *b* = 8.636, and *c* = 12.049 Å for oxalic acid, and *a* = 8.658, *b* = 8.641, and *c* = 12.088 Å for citric acid. These are comparable with the reported values [33]. The oxalic acid leads to a lower lattice volume (888.12 Å³) in comparison with citric acid (900.01 Å³), possibly due to its higher crystallinity. Furthermore, there are no diffraction peaks of carbon in all the patterns due to its amorphous structure and/or the small thickness of the carbon layer on the LVP particles [34]. There are some diffraction peaks related to the Li₃PO₄ phase (PDF no. 00-015-0760) for both samples. The Li₃PO₄ phase is intermediate phase which reacts to form the final Li₃V₂(PO₄)₃ product. Therefore, the existence of impurity Li₃PO₄ phase can be attributed to the low calcination temperature of 800 °C.

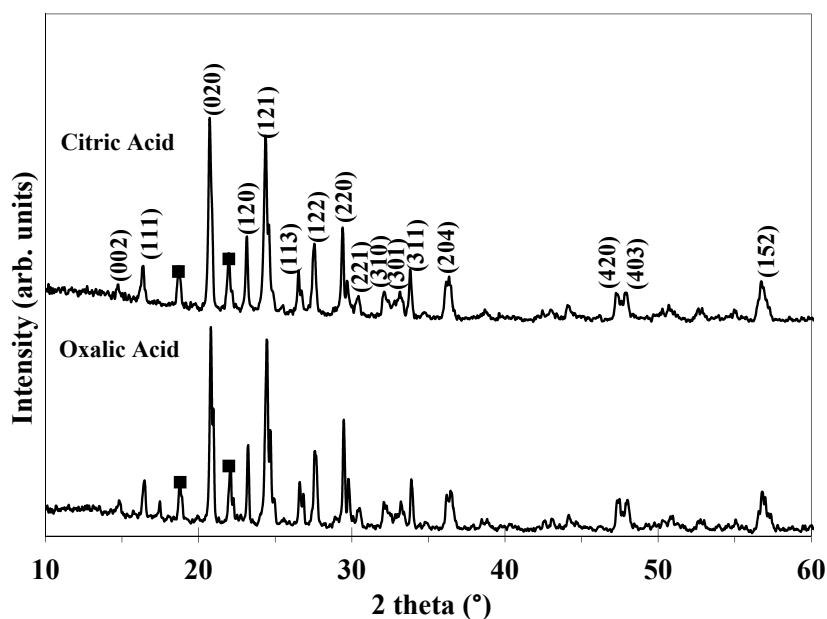


Figure 1. XRD patterns of the Li₃V₂P₃O₁₂ (LVP) compounds obtained by the oxalic and citric acids, Symbol ■ (Li₃PO₄).

The Raman spectroscopy technique was used to identify the existence and nature of carbon in the synthesized LVP powders (Figure 2a). The two characteristic peaks at 1360 cm^{-1} (D-band) and 1560 cm^{-1} (G-band) are assigned to the sp^3 and sp^2 type carbon, respectively [35]. The absence of Raman peaks in the range of $500\text{--}1200\text{ cm}^{-1}$, corresponding to the vibrational mode of $\text{Li}_3\text{V}_2(\text{PO}_4)_3$, is due to the coverage of particle surface by the amorphous carbon layer [36]. The carbon layer enhances the electrical conductivity without affecting the crystallinity of LVP [37]. Furthermore, the carbon layer improves the binding between the carbon additive and LVP in the electrodes. The intensity ratios of D to G band (I_D/I_G) as a criteria of graphitization are higher for oxalic acid (0.94) than for citric acid (0.89), indicating the predominance of sp^2 type carbon domains. The carbon type has the higher contribution on the electrical conductivities. Carbon contents of the LVP particles determined from TGA curves (Figure 2b), are 5.5 wt.% and 4.5 wt.% for oxalic acid and citric acid, respectively. The higher carbon content by the oxalic acid may be due to its lower decomposition temperature.

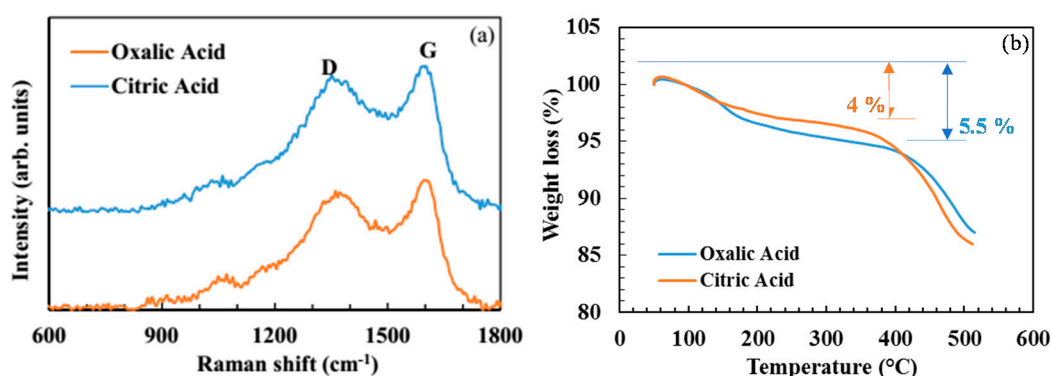


Figure 2. (a) Raman spectra and (b) TGA curves of the LVP compounds.

Figure 3a shows the overall X-ray photoelectron spectroscopy (XPS) examinations of the LVP powder that was synthesized by oxalic acid. The peaks of Li, V, O, P, and C elements are labeled. Figure 3b shows the binding energy of $\text{V}2\text{p}_{3/2}$ and $\text{V}2\text{p}_{1/2}$ at 511.6 and 519.6 eV, respectively.

The observed binding energy values correspond to V^{3+} in LVP, suggesting the successful reduction of V^{5+} to V^{3+} [38]. The binding energy of a characteristic satellite peak of C1s at approximately 280.8 eV (Figure 3c) confirms the existence of carbon [39].

SEM images of the LVP powders prepared by the oxalic acid and citric acid are compared in Figure 4a,c. When used as reducing agents, oxalic acid yields spherical nanoparticles ($\sim 30\text{ nm}$), whereas citric acid yields bulky microstructures containing rod-like particles with a diameter of 50 nm and a length of $0.5\text{ }\mu\text{m}$. The metal precursors are firstly decomposed to the corresponding oxides and phosphates [40–42]. The intermediate solid phases then react to form LVP during the calcination process [43]. The type and amount of metal precursors and organic agents control the decomposition and reaction rates, and therefore, the bulky microstructure can be attributed to the slower decomposition rate in the presence of citric acid caused by its carboxylate groups [44]. The HRTEM images (Figure 4b) clarify the crystal structure of nanoparticles and carbon layer on the particle surface. The interplanar spacing of 0.324 nm correspond to the (122) hkl plane, indicating high crystallinity. Furthermore, the average thickness of the carbon layer is approximately 5 nm . Figure 5 demonstrates that the N_2 adsorption-desorption isotherms of the LVP powders are IV type with a typical H3 hysteresis. The LVP powders prepared by oxalic acid have a lower BET specific surface area ($12\text{ m}^2/\text{g}$) than those of citric acid ($24\text{ m}^2/\text{g}$). The higher pore volume of citric acid ($0.08\text{ cm}^3/\text{g}$) than oxalic acid pore volume ($0.05\text{ cm}^3/\text{g}$) can be attributed to the higher amounts of liberated gases. Furthermore, the pore sizes are mainly distributed at the mesopores range ($1\text{--}20\text{ nm}$) with the maximum at 6.5 nm for the oxalic acid, while the citric acid shows only the micropores ($1\text{--}2\text{ nm}$). The BET specific surface area and pore volume affects the electrochemical properties via tuning the ionic/electronic

conduction pathways and mechanical response during cycling. Furthermore, the pores can partially overcome volume deformation during the Li^+ de-/intercalation from/into the crystal structure [45].

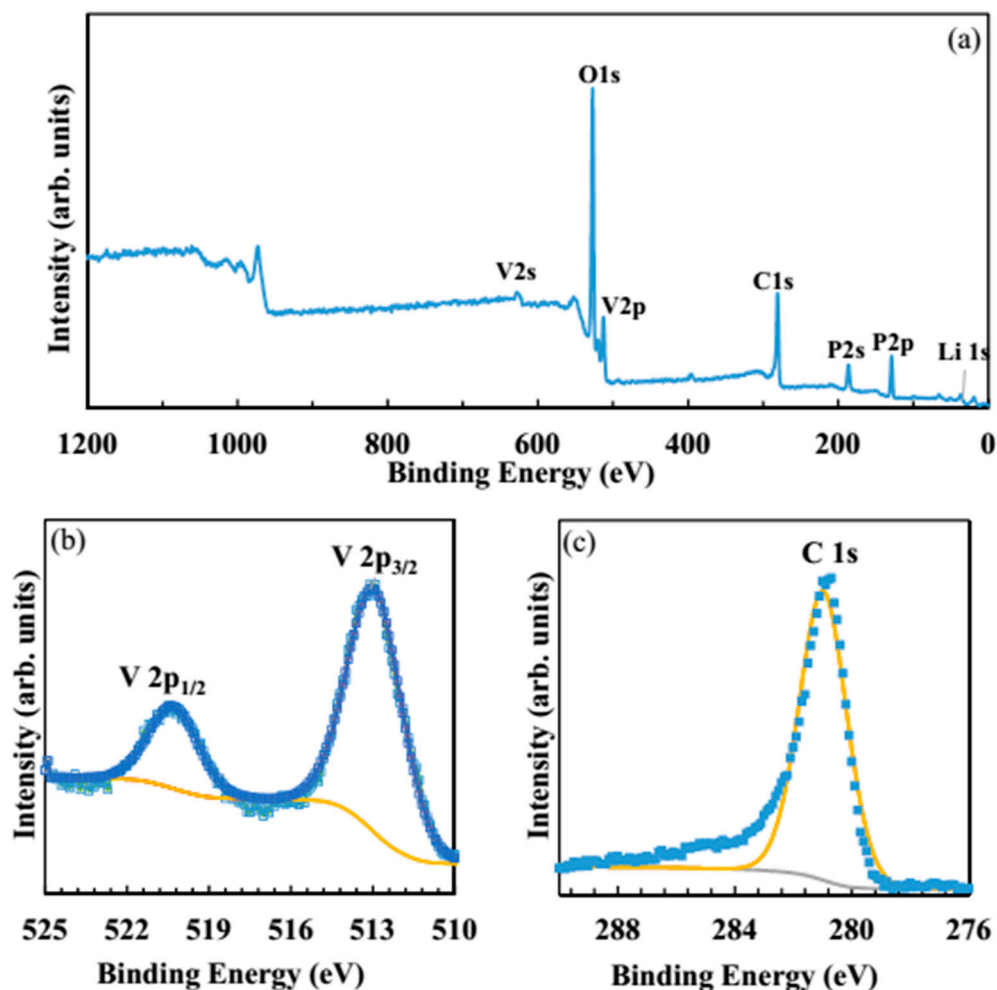


Figure 3. Wide range XPS spectrum showing (a), core level XPS spectra, (b) V2P, and (c) C 1s of the LVP compound prepared by the oxalic acid.

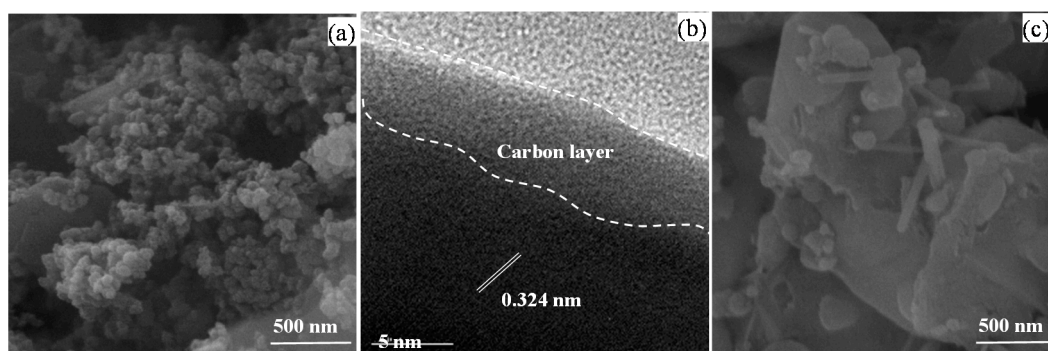


Figure 4. (a) SEM and (b) HRTEM images of the LVP compounds prepared by the oxalic acid and (c) SEM image for the citric acid.

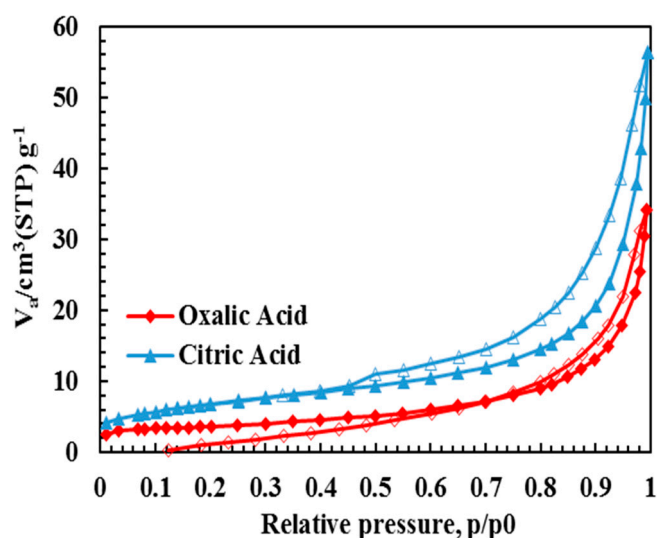
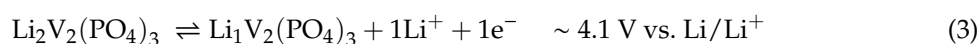
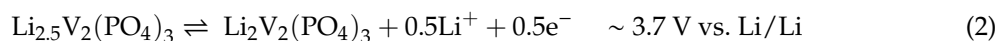
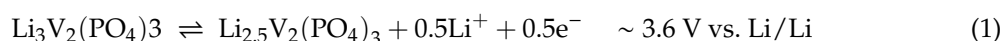


Figure 5. Adsorption (filled symbols)-desorption (open symbols) isotherms of the LVP powders.

Figure 6a,c compare the initial charge/discharge curves of LVP powders at 1C rate and in the range of 3.0–4.3 V. For the oxalic acid, the three charge plateaus are at ~3.63, 3.71, and 4.11 V and three discharge plateaus are at ~3.53, 3.62, and 4.00 V. The citric acid shows the plateaus at 3.62, 3.70, and 4.11 V for the charge process and 3.50, 3.61, and 4.00 V for the discharge process. The voltage plateaus of charge and discharge are related to the reversible phase transition processes, respectively [15,46–49]:



The voltage differences between the charge and discharge plateaus of LVP prepared by oxalic acid are smaller (~260 mV) than those of citric acid (~300 mV), confirming it has less polarization [50]. The initial discharge capacities of oxalic acid and citric acid at 1C are 124 and 123 mAh g⁻¹, respectively, corresponding to 93.2% and 92.4% of the theoretical capacity (~133 mAh g⁻¹) in the range of 3.0–4.3 V. The cycling performances of LVP powders prepared by the oxalic and citric acids at various calcination temperatures and times are summarized in Figure 6b,d. The oxalic acid shows higher and more stable discharge capacities than the citric acid. For the oxalic acid and calcination temperature of 800 °C, the specific discharge capacity of 124 mAh g⁻¹ fades to 123 mAh g⁻¹ after 50 cycles, corresponding to 99% capacity retention. The charge/discharge curves at 50th cycles also confirm the cyclic stability. However, the maximum specific discharge capacity of 122 mAh g⁻¹, together with 99% capacity retention is obtained by the citric acid with the similar calcination process. The discharge capacities and capacity retention decrease with the decrease of calcination temperatures and times, due to the increase of amount of impurity phase and lower crystallinity. Furthermore, the Coulombic efficiencies of oxalic acid are higher than those of citric acid during 1C cycling, indicating the high reversibility of the material [51].

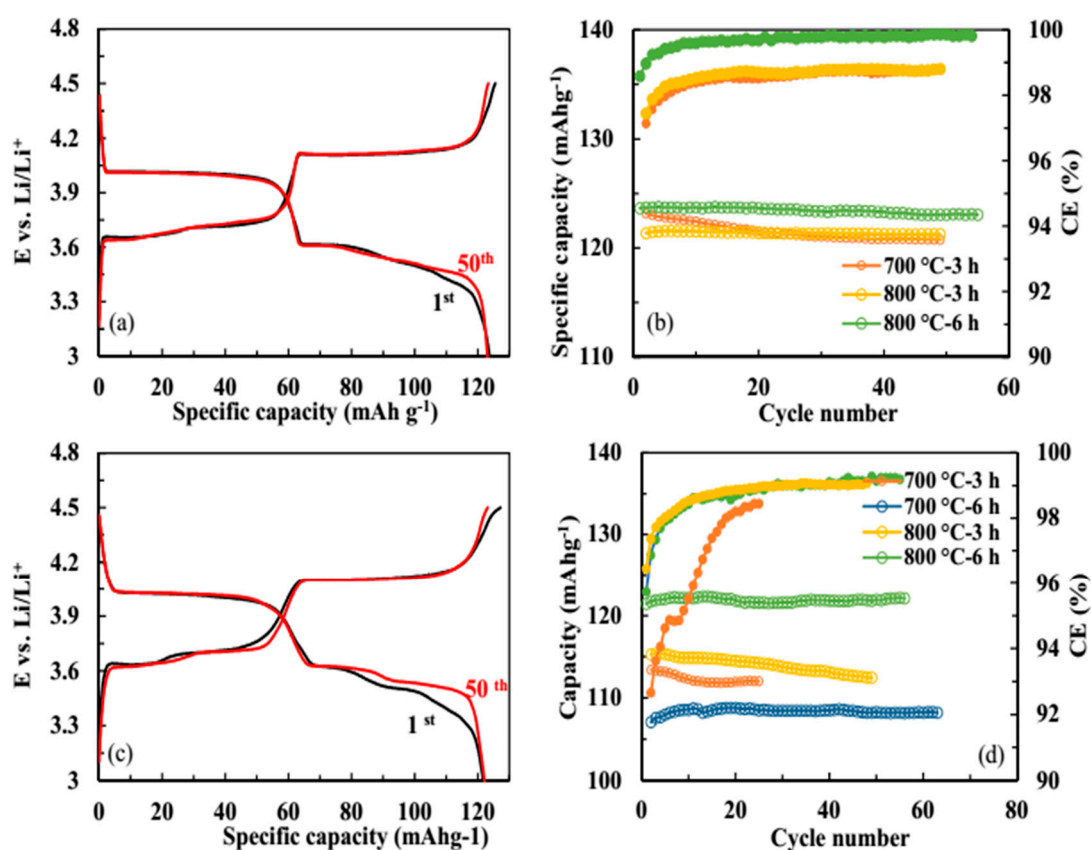


Figure 6. Initial and 50th charge/discharge curves of the LVP compounds prepared by (a) oxalic acid and (c) citric acid and the cyclic performance of the LVP powders prepared by (b) oxalic acid and (d) citric acid, and potential (E) range of 3.0–4.3 V vs. Li.

Figure 7a,b show the charge/discharge curves and cycling performance of the LVP powders prepared by the oxalic acid in the voltage range of 3.0–4.8 V. The four plateaus at approximately 3.68, 3.74, 4.20, and 4.65 V vs. Li/Li⁺ in the charge curves (Figure 7a) correspond to a sequence of phase transitions of Li_xV₂(PO₄)₃, where x = 3.0, 2.5, 2.0, 1.0, and 0 [52–54]. The discharge curve, however, is S-shaped due to solid solution behavior, suggesting a single-phase reaction caused by a disordered lithium reinsertion [16]. With sufficient Li⁺ reinsertion, the two-phase behavior reappears for the reinsertion of the third lithium [55]. The capacity fading in the range of 3.0–4.8 V is more notable during long-term cycling than in the range of 3.0–4.3 V, which can be attributed to structural collapse during the phase transition from V₂(PO₄)₃ to LiV₂(PO₄)₃ in a solid solution regime at upper voltage of 4.8 V, as can be observed in the charge/discharge curves [56].

The rate performance of the LVP powders prepared by the oxalic acid and calcined at 800 °C is presented in Figure 7c,d. With the rapid current rate increase, the stable discharge capacity is obtained at each state. When the rate gradually increases from 0.1 to 1, 3, 5, and 10 C, the average discharge capacities decrease from 122.5 to 116.9, 90.9, 63.8, and 6.3 mAh g⁻¹, respectively. The discharge capacity returns to 126.2 mAh g⁻¹ when the current density returns to 0.1 C, indicating good rate capability of the synthesized LVP powders. This is explainable by the small spherical nanoparticles and carbon layer on the LVP particles, thereby improving the electronic conductivity [57]. Figure 7d shows that the voltage plateaus are degraded with the increased current densities. The charge/discharge curves reappear, however, by decreasing the current density to 0.1 C, indicating both structural and electrochemical stability at the higher current densities, in addition to the sufficient electron/ion conductivity of the synthesized LVP powders.

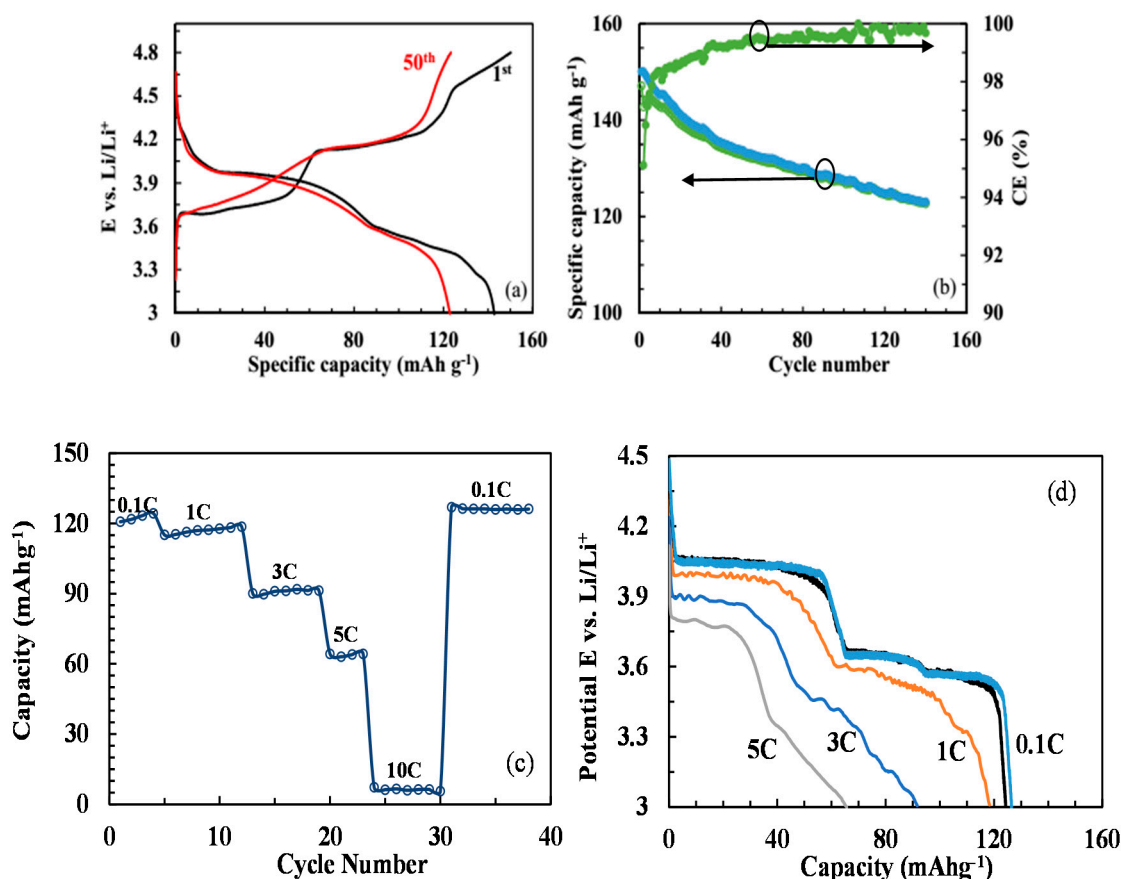


Figure 7. (a) Initial and 50 th charge/discharge curves, (b) cyclic performance, (c) rate performance and (d) charge/discharge curves of the LVP compounds prepared by the oxalic acid in the potential (E) range of 3.0–4.8 V Vs. Li.

Figure 8 compares the cyclic voltammetry curves of LVP powders at 0.1 mVs^{-1} in the voltage range of 3.0–4.8 V and the Nyquist plots. The LVP powders prepared by the oxalic acid have a high redox current and a large curve area. There are four peaks at 3.61, 3.71, 4.12, and 4.61 V in the charge process and three peaks at 3.59, 3.65, and 3.90 V in the discharge process, showing the reversible phase transitions during the Li-ion extraction/insertion [58]. The potential peaks at ~ 4.12 and 4.61 V appear as a single peak at ~ 3.90 V during the discharge process. This is attributed to the solid solution region from $\text{V}_2(\text{PO}_4)_3$ to $\text{Li}_2\text{V}_2(\text{PO}_4)_3$ [59]. The results are in good agreement with the charge/discharge curves (Figures 7a and 8b), showing the superior electrochemical properties of the LVP powders synthesized using the oxalic acid as the reducing agent. The impedance spectra consisted of a semicircle and a linear part at high and low frequency ranges, respectively. The diameter of the semicircle shows the combination of surface film (R_{sf}) + charge transfer resistance (R_{ct}) and corresponding capacitance due to surface film (CPE_{sf}) and double layer (CPE_{dl}) which mainly affects the cathode impedance [6,60]. The smaller diameter of the semicircle for the oxalic acid (95Ω) than the diameter of the semicircle for the citric acid (112Ω) confirms its smaller $R_{(sf+ct)}$ resistance [61]. We also note Warburg region clearly noted when compared to our previous impedance studies of other cathode and anode materials [6,62–65], further careful studies on impedance studies at various voltages during charge and discharge cycle and cycle number are needed.

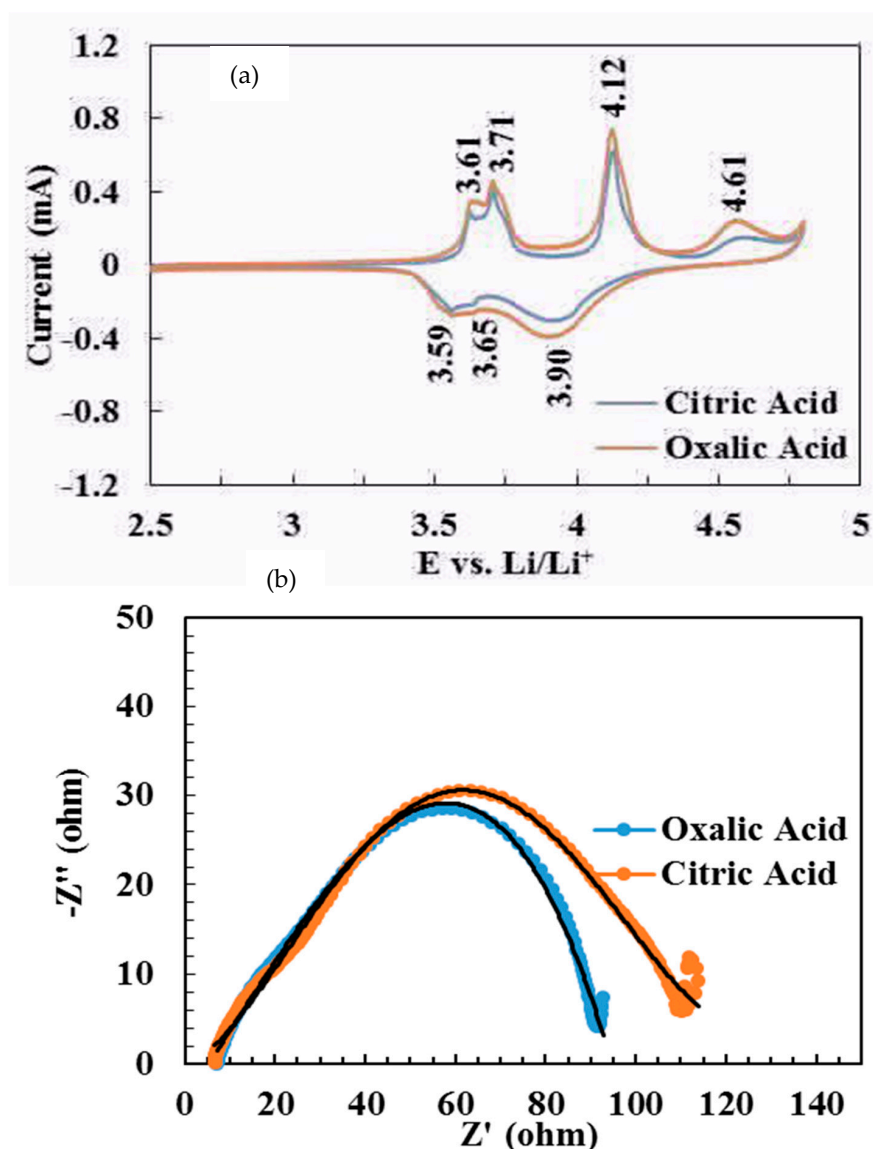


Figure 8. (a) Cyclic voltammograms of $\text{Li}_3\text{V}_2\text{P}_3\text{O}_{12}$ (LVP) prepared using two precursors. Scan rate, 0.1 mVs^{-1} , for clarity second cycle are shown, Li metal as counter and reference electrode, and (b) Nyquist plots (Z' vs. $-Z''$) of LVP electrodes.

Table 1 compares the discharge capacity and retention of various $\text{Li}_3\text{V}_2(\text{PO}_4)_3$ cathode materials. It is worth to note that the $\text{Li}_3\text{V}_2(\text{PO}_4)_3/\text{C}$ samples synthesized by the oxalic acid show the comparable discharge capacity and cycling performance in the voltage range of 3.0–4.3 V vs. Li^+/Li .

Table 1. Summary of electrochemical properties of $\text{Li}_3\text{V}_2(\text{PO}_4)_3/\text{C}$ cathode material.

Material	Synthesis Method	Capacity (mAh g^{-1} , at 1C Rate)	Retention (%)	Reference
$\text{Li}_3\text{V}_2(\text{PO}_4)_3/\text{RGO}$	Solvothermal	128, 1C	98	[18]
$\text{Li}_3\text{V}_2(\text{PO}_4)_3/\text{C}$	Solvothermal	112, 1C	97	[20]
$\text{Li}_3\text{V}_2(\text{PO}_4)_3$ in carbon matrix	Solvothermal	122, 1C	100	[21]
$\text{Li}_3\text{V}_2(\text{PO}_4)_3/\text{C}$	Microemulsion	130, 1C	97	[22]
$\text{Li}_3\text{V}_2(\text{PO}_4)_3/\text{C}$	Solution synthesis	130, 0.2C	93	[24]
$\text{Li}_3\text{V}_2(\text{PO}_4)_3/\text{C}$	Solvothermal	122, 1.5C	98	[26]
$\text{Li}_3\text{V}_2(\text{PO}_4)_3/\text{C}$	Freeze-drying	130, 0.1C	98	[27]
$\text{Li}_3\text{V}_2(\text{PO}_4)_3/\text{C}$	Microwave	130, 1C	99	[29]
$\text{Li}_3\text{V}_2(\text{PO}_4)_3/\text{C}$	Solution synthesis	124, 1C	98	This work

4. Conclusions

The dependency of structural, microstructure, and electrochemical properties of $\text{Li}_3\text{V}_2(\text{PO}_4)_3$ powders were examined as a function of reducing agent and calcination temperatures (700 and 800 °C) and times (3 and 6 h). The smaller particle size obtained by means of the oxalic acid led to a lower charge-transfer resistance (95 Ω) compared with that for the citric acid (112 Ω). Following calcination at 800 °C for 6 h, the LVP powders synthesized by the oxalic acid showed the highest specific discharge capacity of 122.5 mAhg^{-1} at 1C and higher cycling performance (capacity retention of 99.8% following 55 cycles). With decreased calcination temperatures and times, the specific capacity faded during cycling and the Columbic efficiencies decreased due to the decreased crystallinity. The better electrochemical performance achieved by oxalic acid was mainly attributed to its smaller spherical nanoparticles. Further studies are needed on the applicability of this material with solid electrolyte for all solid State Batteries [66].

Author Contributions: A.Y., Data curation, Formal analysis, A.S., Data curation, Formal analysis. M.V.R., Supervision, Investigation, Project administration, editing, S.M.M., Supervision, Conceptualization, Writing—review & editing. M.H., Supervision, Conceptualization, Writing—review & editing. D.S., Investigation, C.K.O., Funding acquisition. S.A., Resources; Editing. All authors have read and agreed to the published version of the manuscript.

Funding: Authors thank to National University of Singapore for support.

Conflicts of Interest: The Authors declare no conflict of interest.

References

1. Mauger, A.; Julien, C.; Paoletta, A.; Armand, M.; Zaghbi, K. Recent progress on organic electrodes materials for rechargeable batteries and supercapacitors. *Materials* **2019**, *12*, 1770. [[CrossRef](#)] [[PubMed](#)]
2. Reddy, M.V.; Subba Rao, G.V.; Chowdari, B.V.R. Metal Oxides and Oxysalts as Anode Materials for Li Ion Batteries. *Chem. Rev.* **2013**, *113*, 5364–5457. [[CrossRef](#)] [[PubMed](#)]
3. Dickens, P.G.; French, S.J.; Hight, A.T.; Pye, M.F. Phase relationships in the ambient temperature $\text{Li}_x\text{V}_2\text{O}_5$ system ($0.1 < x < 1.0$). *Mater. Res. Bull.* **1979**, *14*, 1295–1299.
4. Reddy, M.V.; Mauger, A.; Julien, C.M.; Paoletta, A.; Zaghbi, K.J.M. Brief History of Early Lithium-Battery Development. *Materials* **2020**, *13*, 1884. [[CrossRef](#)]
5. Barker, J.; Saidi, M.Y.; Swoyer, J.L. Electrochemical insertion properties of the novel lithium vanadium fluorophosphate, LiVPO_4F . *J. Electrochem. Soc.* **2003**, *150*, A1394–A1398. [[CrossRef](#)]
6. Reddy, M.V.; Subba Rao, G.V.; Chowdari, B.V.R. Long-term cycling studies on 4V-cathode, lithium vanadium fluorophosphate. *J. Power Sources* **2010**, *195*, 5768–5774. [[CrossRef](#)]
7. Nagarathinam, M.; Saravanan, K.; Phua, E.J.H.; Reddy, M.V.; Chowdari, B.V.R.; Vittal, J.J. Redox-Active Metal-Centered Oxalato Phosphate Open Framework Cathode Materials for Lithium Ion Batteries. *Angew. Chem. Int. Ed.* **2012**, *51*, 5866–5870. [[CrossRef](#)]
8. Hameed, A.S.; Nagarathinam, M.; Schreyer, M.; Reddy, M.V.; Chowdari, B.V.R.; Vittal, J.J. A layered oxalato-phosphate framework as a cathode material for Li-ion batteries. *J. Mater. Chem. A* **2013**, *1*, 5721–5726. [[CrossRef](#)]
9. Hameed, A.S.; Reddy, M.V.; Nagarathinam, M.; Runčevski, T.; Dinnebier, R.E.; Adams, S.; Chowdari, B.V.R.; Vittal, J.J. Room temperature large-scale synthesis of layered frameworks as low-cost 4V cathode materials for lithium ion batteries. *Sci. Rep.* **2015**, *5*, 16270. [[CrossRef](#)]
10. Hameed, A.S.; Reddy, M.V.; Sarkar, N.; Chowdari, B.V.R.; Vittal, J.J. Synthesis and electrochemical investigation of novel phosphite based layered cathodes for Li-ion batteries. *RSC Adv.* **2015**, *5*, 60630–60637. [[CrossRef](#)]
11. Shahul Hameed, A.; Nagarathinam, M.; Reddy, M.V.; Chowdari, B.V.R.; Vittal, J.J. Synthesis and electrochemical studies of layer-structured metastable alpha LiVOPO_4 . *J. Mater. Chem.* **2012**, *22*, 7206–7213. [[CrossRef](#)]
12. Saidi, M.Y.; Barker, J.; Huang, H.; Swoyer, J.L.; Adamson, G. Electrochemical properties of lithium vanadium phosphate as a cathode material for lithium-ion batteries. *Electrochem. Solid State Lett.* **2002**, *5*, A149–A151. [[CrossRef](#)]

13. Sakunthala, A.; Reddy, M.V.; Selvasekarapandian, S.; Chowdari, B.V.R.; Selvin, P.C. Preparation, Characterization, and Electrochemical Performance of Lithium Trivanadate Rods by a Surfactant-Assisted Polymer Precursor Method for Lithium Batteries. *J. Phys. Chem. C* **2010**, *114*, 8099–8107. [[CrossRef](#)]
14. Tan, H.; Xu, L.; Geng, H.; Rui, X.; Li, C.; Huang, S. Nanostructured $\text{Li}_3\text{V}_2(\text{PO}_4)_3$ Cathodes. *Small* **2018**, *14*, 1800567. [[CrossRef](#)] [[PubMed](#)]
15. Liu, C.; Massé, R.; Nan, X.; Cao, G. A promising cathode for Li-ion batteries: $\text{Li}_3\text{V}_2(\text{PO}_4)_3$. *Energy Storage Mater.* **2016**, *4*, 15–58. [[CrossRef](#)]
16. Rui, X.; Yan, Q.; Skyllas-Kazacos, M.; Lim, T.M. $\text{Li}_3\text{V}_2(\text{PO}_4)_3$ cathode materials for lithium-ion batteries: A review. *J. Power Sources* **2014**, *258*, 19–38. [[CrossRef](#)]
17. Membreno, N.; Park, K.; Goodenough, J.B.; Stevenson, K.J. Electrode/Electrolyte Interface of Composite $\alpha\text{-Li}_3\text{V}_2(\text{PO}_4)_3$ Cathodes in a Nonaqueous Electrolyte for Lithium Ion Batteries and the Role of the Carbon Additive. *Chem. Mater.* **2015**, *27*, 3332–3340. [[CrossRef](#)]
18. Pei, B.; Jiang, Z.; Zhang, W.; Yang, Z.; Manthiram, A. Nanostructured $\text{Li}_3\text{V}_2(\text{PO}_4)_3$ cathode supported on reduced graphene oxide for lithium-ion batteries. *J. Power Sources* **2013**, *239*, 475–482. [[CrossRef](#)]
19. Gaubicher, J.; Wurm, C.; Goward, G.; Masquelier, C.; Nazar, L. Rhombohedral Form of $\text{Li}_3\text{V}_2(\text{PO}_4)_3$ as a Cathode in Li-Ion Batteries. *Chem. Mater.* **2000**, *12*, 3240–3242. [[CrossRef](#)]
20. Yu, S.; Mertens, A.; Kungl, H.; Schierholz, R.; Tempel, H.; Eichel, R.-A. Morphology Dependency of $\text{Li}_3\text{V}_2(\text{PO}_4)_3/\text{C}$ Cathode Material Regarding to Rate Capability and Cycle Life in Lithium-ion Batteries. *Electrochim. Acta* **2017**, *232*, 310–322. [[CrossRef](#)]
21. Zhang, X.; Kühnel, R.-S.; Hu, H.; Eder, D.; Balducci, A. Going nano with protic ionic liquids—The synthesis of carbon coated $\text{Li}_3\text{V}_2(\text{PO}_4)_3$ nanoparticles encapsulated in a carbon matrix for high power lithium-ion batteries. *Nano Energy* **2015**, *12*, 207–214. [[CrossRef](#)]
22. Wang, S.; Zhang, Z.; Deb, A.; Yang, C.; Yang, L.; Hirano, S.-I. Nanostructured $\text{Li}_3\text{V}_2(\text{PO}_4)_3/\text{C}$ composite as high-rate and long-life cathode material for lithium ion batteries. *Electrochim. Acta* **2014**, *143*, 297–304. [[CrossRef](#)]
23. Son, J.N.; Kim, S.H.; Kim, M.C.; Kim, G.J.; Aravindan, V.; Lee, Y.G.; Lee, Y.S. Superior charge-transfer kinetics of NASICON-type $\text{Li}_3\text{V}_2(\text{PO}_4)_3$ cathodes by multivalent Al^{3+} and Cl^- substitutions. *Electrochim. Acta* **2013**, *97*, 210–215. [[CrossRef](#)]
24. Zhang, S.; Gu, Q.; Tan, S.; Zhao, L. Improved electrochemical properties of the $\text{Li}_3\text{V}_2(\text{PO}_4)_3$ cathode material synthesized from a V(III) precursor. *J. Alloy. Compd.* **2019**, *802*, 583–590. [[CrossRef](#)]
25. Yang, Z.; Hu, J.; Chen, Z.; Zhong, J.; Gu, N.; Zhang, N. Sol-gel-assisted, fast and low-temperature synthesis of La-doped $\text{Li}_3\text{V}_2(\text{PO}_4)_3/\text{C}$ cathode materials for lithium-ion batteries. *RSC Adv.* **2015**, *5*, 17924–17930. [[CrossRef](#)]
26. Wang, L.; Bai, J.; Gao, P.; Wang, X.; Looney, J.P.; Wang, F. Structure Tracking Aided Design and Synthesis of $\text{Li}_3\text{V}_2(\text{PO}_4)_3$ Nanocrystals as High-Power Cathodes for Lithium Ion Batteries. *Chem. Mater.* **2015**, *27*, 5712–5718. [[CrossRef](#)]
27. Guo, S.; Bai, Y.; Geng, Z.; Wu, F.; Wu, C. Facile synthesis of $\text{Li}_3\text{V}_2(\text{PO}_4)_3/\text{C}$ cathode material for lithium-ion battery via freeze-drying. *J. Energy Chem.* **2019**, *32*, 159–165. [[CrossRef](#)]
28. Zheng, L.-L.; Xue, Y.; Liu, B.-S.; Zhou, Y.-X.; Hao, S.-E.; Wang, Z.-B. High performance $\text{Na}_3\text{V}_2(\text{PO}_4)_3$ cathode prepared by a facile solution evaporation method for sodium-ion batteries. *Ceram. Int.* **2017**, *43*, 4950–4956. [[CrossRef](#)]
29. Xi, Y.; Zhang, Y.; Su, Z. Microwave synthesis of $\text{Li}_3\text{V}_2(\text{PO}_4)_3/\text{C}$ as positive-electrode materials for rechargeable lithium batteries. *J. Alloy. Compd.* **2015**, *628*, 396–400. [[CrossRef](#)]
30. Ou, Q.-Z.; Tang, Y.; Zhong, Y.-J.; Guo, X.-D.; Zhong, B.-H.; Heng, L.; Chen, M.-Z. Submicrometer porous $\text{Li}_3\text{V}_2(\text{PO}_4)_3/\text{C}$ composites with high rate electrochemical performance prepared by sol-gel combustion method. *Electrochim. Acta* **2014**, *137*, 489–496. [[CrossRef](#)]
31. Hameed, A.S.; Reddy, M.V.; AlQaradawi, S.Y.; Adams, S. Synthesis, structural and lithium storage studies of graphene- LiVSi_2O_6 composites. *Ionics* **2019**, *25*, 1559–1566. [[CrossRef](#)]
32. Tan, T.Q.; Idris, M.S.; Osman, R.A.M.; Reddy, M.V.; Chowdari, B.V.R. Structure and electrochemical behaviour of $\text{LiNi}_{0.4}\text{Mn}_{0.4}\text{Co}_{0.2}\text{O}_2$ as cathode material for lithium ion batteries. *Solid State Ion.* **2015**, *278*, 43–48. [[CrossRef](#)]
33. Dai, C.; Chen, Z.; Jin, H.; Hu, X. Synthesis and performance of $\text{Li}_3(\text{V}_{1-x}\text{Mg}_x)_2(\text{PO}_4)_3$ cathode materials. *J. Power Sources* **2010**, *195*, 5775–5779. [[CrossRef](#)]

34. Shin, H.C.; Cho, W.I.; Jang, H. Electrochemical properties of the carbon-coated LiFePO₄ as a cathode material for lithium-ion secondary batteries. *J. Power Sources* **2006**, *159*, 1383–1388. [[CrossRef](#)]
35. Ferrari, A.C.; Robertson, J. Interpretation of Raman spectra of disordered and amorphous carbon. *Phys. Rev. B* **2000**, *61*, 14095–14107. [[CrossRef](#)]
36. Chen, J.; Zhao, N.; Guo, F.-F. Impact of carbon coating thickness on the electrochemical properties of Li₃V₂(PO₄)₃/C composites. *Russ. J. Electrochem.* **2017**, *53*, 339–344. [[CrossRef](#)]
37. Wang, J.; Zhang, X.; Liu, J.; Yang, G.; Ge, Y.; Yu, Z.; Wang, R.; Pan, X. Long-term cyclability and high-rate capability of Li₃V₂(PO₄)₃/C cathode material using PVA as carbon source. *Electrochim. Acta* **2010**, *55*, 6879–6884. [[CrossRef](#)]
38. Cao, Y.; Liu, Y.; Chen, T.; Xia, X.; Zhang, L.-C.; Zhang, J.; Xia, Y. Na₃V₂(PO₄)₃ nanoparticles confined in functional carbon framework towards high-rate and ultralong-life sodium storage. *J. Alloy. Compd.* **2019**, *791*, 296–306. [[CrossRef](#)]
39. He, W.; Zhang, X.; Jin, C.; Wang, Y.; Mossin, S.; Yue, Y. Nano-glass ceramic cathodes for Li⁺/Na⁺ mixed-ion batteries. *J. Power Sources* **2017**, *342*, 717–725. [[CrossRef](#)]
40. Varma, A.; Mukasyan, A.S.; Rogachev, A.S.; Manukyan, K.V. Solution Combustion Synthesis of Nanoscale Materials. *Chem. Rev.* **2016**, *116*, 14493–14586. [[CrossRef](#)]
41. Wen, W.; Wu, J.-M. Nanomaterials via solution combustion synthesis: A step nearer to controllability. *RSC Adv.* **2014**, *4*, 58090–58100. [[CrossRef](#)]
42. Li, F.-T.; Ran, J.; Jaroniec, M.; Qiao, S.Z. Solution combustion synthesis of metal oxide nanomaterials for energy storage and conversion. *Nanoscale* **2015**, *7*, 17590–17610. [[CrossRef](#)] [[PubMed](#)]
43. Haghi, Z.; Masoudpanah, S.M. Technology, CTAB-assisted solution combustion synthesis of LiFePO₄ powders. *J. Sol. Gel. Sci. Technol.* **2019**, *91*, 335–341. [[CrossRef](#)]
44. Erri, P.; Pranda, P.; Varma, A. Oxidizer–Fuel Interactions in Aqueous Combustion Synthesis. 1. Iron(III) Nitrate–Model Fuels. *Ind. Eng. Chem. Res.* **2004**, *43*, 3092–3096. [[CrossRef](#)]
45. Liu, X.; Feng, X.; Xu, X.; Wang, F.; Wang, Y.J.J. Technology, Sol-assisted spray-drying synthesis of porous Li₃V₂(PO₄)₃/C microspheres as high-activity cathode materials for lithium-ion batteries. *J. Sol. Gel. Sci. Technol.* **2018**, *86*, 343–350. [[CrossRef](#)]
46. Morcrette, M.; Leriche, J.-B.; Patoux, S.; Wurm, C.; Masquelier, C. In Situ X-Ray Diffraction during Lithium Extraction from Rhombohedral and Monoclinic Li₃V₂(PO₄)₃. *Electrochem. Solid State Lett.* **2003**, *6*, A80–A84. [[CrossRef](#)]
47. Yu, S.; Mertens, A.; Schierholz, R.; Gao, X.; Aslanbas, Ö.; Mertens, J.; Kungl, H.; Tempel, H.; Eichel, R.-A. An Advanced All Phosphate Lithium-Ion Battery Providing High Electrochemical Stability, High Rate Capability and Long-Term Cycling Performance. *J. Electrochem. Soc.* **2017**, *164*, A370–A379. [[CrossRef](#)]
48. Xu, W.; Liu, L.; Guo, H.; Guo, R.; Wang, C. Synthesis and electrochemical properties of Li₃V₂(PO₄)₃/C cathode material with an improved sol–gel method by changing pH value. *Electrochim. Acta* **2013**, *113*, 497–504. [[CrossRef](#)]
49. Hameed, A.S.; Reddy, M.V.; Chowdari, B.V.R.; Vittal, J.J. Carbon coated Li₃V₂(PO₄)₃ from the single-source precursor, Li₂(VO)₂(HPO₄)₂(C₂O₄).6H₂O as cathode and anode materials for Lithium ion batteries. *Electrochim. Acta* **2014**, *128*, 184–191. [[CrossRef](#)]
50. Hu, G.; Gan, Z.; Cao, Y.; Peng, Z.; Lu, Y.; Du, K. Multi-level carbon co-modified LiVPO₄F cathode material for lithium batteries. *J. Alloy. Compd.* **2019**, *788*, 1146–1153. [[CrossRef](#)]
51. Yang, F.; Wang, D.; Zhao, Y.; Tsui, K.-L.; Bae, S.J. A study of the relationship between coulombic efficiency and capacity degradation of commercial lithium-ion batteries. *Energy* **2018**, *145*, 486–495. [[CrossRef](#)]
52. Yan, J.; Fang, H.; Jia, X.; Wang, L. Copper incorporated in Li₃V₂(PO₄)₃/C cathode materials and its effects on high-rate Li-ion batteries. *J. Alloy. Compd.* **2018**, *730*, 103–109. [[CrossRef](#)]
53. Xia, A.; Huang, J.; Tan, G.; Ren, H. Synthesis and electrochemical properties of W-doped Li₃V₂(PO₄)₃/C cathode materials for lithium ion batteries. *Ceram. Int.* **2014**, *40*, 14845–14850. [[CrossRef](#)]
54. Cao, Z.; Fang, T.; Hou, X.; Niu, J. In-situ preparation of nitrogen-doped carbon-modified lithium vanadium phosphate fibers with mesoporous nanostructure for lithium energy storage. *Ceram. Int.* **2019**, *45*, 14474–14478. [[CrossRef](#)]
55. Wang, J.; Zheng, S.; Hojamberdiev, M.; Ren, B.; Xu, Y.; Shao, C. Effect of Ni doping on electrochemical performance of Li₃V₂(PO₄)₃/C cathode material prepared by polyol process. *Ceram. Int.* **2014**, *40*, 11251–11259. [[CrossRef](#)]

56. Xu, K. Electrolytes and Interphases in Li-Ion Batteries and Beyond. *Chem. Rev.* **2014**, *114*, 11503–11618. [[CrossRef](#)]
57. Du, X.; He, W.; Zhang, X.; Yue, Y.; Liu, H.; Zhang, X.; Min, D.; Ge, X.; Du, Y. Enhancing the electrochemical performance of lithium ion batteries using mesoporous $\text{Li}_3\text{V}_2(\text{PO}_4)_3/\text{C}$ microspheres. *J. Mater. Chem.* **2012**, *22*, 5960–5969. [[CrossRef](#)]
58. Jiang, S. Fabrication and characterization of plate-like $\text{Li}_3\text{V}_2(\text{PO}_4)_3/\text{C}$ as cathode material for energy storage. *Solid State Ion.* **2018**, *325*, 128–132. [[CrossRef](#)]
59. Zhang, C.; Shen, L.; Li, H.; Ping, N.; Zhang, X. Enhanced electrochemical properties of MgF_2 and C co-coated $\text{Li}_3\text{V}_2(\text{PO}_4)_3$ composite for Li-ion batteries. *J. Electroanal. Chem.* **2016**, *762*, 1–6. [[CrossRef](#)]
60. Li, W.; Zheng, H.; Chu, G.; Luo, F.; Zheng, J.; Xiao, D.; Li, X.; Gu, L.; Li, H.; Wei, X.; et al. Effect of electrochemical dissolution and deposition order on lithium dendrite formation: A top view investigation. *Faraday Discuss.* **2014**, *176*, 109–124. [[CrossRef](#)]
61. Tang, S.B.; Lai, M.O.; Lu, L. Li-ion diffusion in highly (003) oriented LiCoO_2 thin film cathode prepared by pulsed laser deposition. *J. Alloy. Compd.* **2008**, *449*, 300–303. [[CrossRef](#)]
62. Das, B.; Reddy, M.V.; Subba Rao, G.V.; Chowdari, B.V.R. Nano-phase tin hollandites, $\text{K}_2(\text{M}_2\text{Sn}_6)\text{O}_{16}$ (M = Co, In) as anodes for Li-ion batteries. *J. Mater. Chem.* **2011**, *21*, 1171–1180. [[CrossRef](#)]
63. Reddy, M.V.; Jose, R.; Le Viet, A.; Ozoemena, K.I.; Chowdari, B.V.R.; Ramakrishna, S. Studies on the lithium ion diffusion coefficients of electrospun Nb_2O_5 nanostructures using galvanostatic intermittent titration and electrochemical impedance spectroscopy. *Electrochim. Acta* **2014**, *128*, 198–202. [[CrossRef](#)]
64. Reddy, M.V.; Prithvi, G.; Loh, K.P.; Chowdari, B.V.R. Li storage and impedance spectroscopy studies on Co_3O_4 , CoO , and CoN for Li-ion batteries. *ACS Appl. Mater. Interfaces* **2014**, *6*, 680–690. [[CrossRef](#)]
65. Reddy, M.V.; Wen, B.L.W.; Loh, K.P.; Chowdari, B.V.R. Energy Storage Studies on InVO_4 as High Performance Anode Material for Li-Ion Batteries. *ACS Appl. Mater. Interfaces* **2013**, *5*, 7777–7785. [[CrossRef](#)] [[PubMed](#)]
66. Reddy, M.V.; Julien, C.M.; Mauger, A.; Zaghbi, K.J.M. Sulfide and Oxide Inorganic Solid Electrolytes for All-Solid-State Li Batteries: A Review. *Nanomaterials* **2020**, *10*, 1606. [[CrossRef](#)]



© 2020 by the authors. Licensee MDPI, Basel, Switzerland. This article is an open access article distributed under the terms and conditions of the Creative Commons Attribution (CC BY) license (<http://creativecommons.org/licenses/by/4.0/>).